

This discussion paper is/has been under review for the journal Atmospheric Chemistry and Physics (ACP). Please refer to the corresponding final paper in ACP if available.

Climatic impacts of stratospheric geoengineering with sulfate, black carbon and titania injection

A. C. Jones¹, J. M. Haywood^{1,2}, and A. Jones²

¹College of Engineering Maths and Physical Sciences, University of Exeter, Exeter, UK

²Met Office Hadley Centre, Exeter, UK

Received: 12 October 2015 – Accepted: 13 October 2015 – Published: 3 November 2015

Correspondence to: A. C. Jones (aj247@exeter.ac.uk)

Published by Copernicus Publications on behalf of the European Geosciences Union.

Climatic impacts of stratospheric geoengineering with sulfate, black carbon and titania injection

A. C. Jones et al.

Title Page

Abstract

Introduction

Conclusions

References

Tables

Figures

◀

▶

◀

▶

Back

Close

Full Screen / Esc

Printer-friendly Version

Interactive Discussion

Abstract

In this paper, we examine the potential climatic effects of geoengineering by sulfate, black carbon and titania injection against a baseline RCP8.5 scenario. We use the HadGEM2-CCS model to simulate scenarios in which the top-of-the-atmosphere radiative imbalance due to rising greenhouse gas concentrations is offset by sufficient aerosol injection throughout the 2020–2100 period. We find that the global-mean temperature is effectively maintained at historical levels for the entirety of the period for all 3 aerosol-injection scenarios, though there are a wide range of side-effects which are discussed in detail. The most prominent conclusion is that although the BC injection rate necessary to produce an equivalent global mean temperature-response is much lower, the severity of stratospheric temperature changes ($> +70^{\circ}\text{C}$) and precipitation impacts effectively exclude BC from being a viable option for geoengineering. Additionally, while it has been suggested that titania would be an effective particle because of its high scattering efficiency, it also efficiently absorbs solar ultraviolet radiation producing a significant stratospheric warming ($> +20^{\circ}\text{C}$). As injection rates for titania are close to those for sulfate, there appears little benefit of using titania when compared to injection of sulfur dioxide, which has the added benefit of being well modelled through extensive research that has been carried out on naturally occurring explosive volcanic eruptions.

1 Introduction

The climatic impacts of continued greenhouse gas (GHG) emissions are likely to be severe which has prompted countenance of new strategies for tackling GHG-induced global warming (e.g Collins et al., 2014). Geoengineering strategies, or large-scale climate interventions that aim to reduce global warming, include strategies to sequester atmospheric carbon dioxide – Carbon Dioxide Removal (CDR) methods, and strategies to reduce solar irradiance at Earth’s surface – Solar Radiation Manage-

Climatic impacts of stratospheric geoengineering with sulfate, black carbon and titania injection

A. C. Jones et al.

Title Page

Abstract

Introduction

Conclusions

References

Tables

Figures



Back

Close

Full Screen / Esc

Printer-friendly Version

Interactive Discussion



Climatic impacts of stratospheric geoengineering with sulfate, black carbon and titania injection

A. C. Jones et al.

Title Page

Abstract

Introduction

Conclusions

References

Tables

Figures

◀

▶

◀

▶

Back

Close

Full Screen / Esc

Printer-friendly Version

Interactive Discussion

ment (SRM) methods (Shepherd et al., 2009). Stratospheric Aerosol Injection (SAI), an SRM scheme which has received significant attention, involves the enhancement of the stratospheric aerosol layer in order to reflect more sunlight back to space. This scheme mimics large volcanic eruptions such as Mt. Pinatubo in 1991, which injected approximately 15–20 Tg of sulfur dioxide (SO₂) into the tropical stratosphere and induced a globally averaged surface cooling of around −0.3 °C for the following two years (Stenchikov et al., 2002).

Sulfate (SO₄) aerosols have featured predominantly in SAI research because of the volcanic analogue (e.g. in the Geoengineering Model Intercomparison Project, GeoMIP, Kravitz et al., 2013). General Circulation Model (GCM) simulations suggest that, while sufficient sulfate injection could effectively reduce global-mean temperature, possible side effects include changes to regional precipitation (e.g. Bala et al., 2008; Tilmes et al., 2013), ozone (e.g. Tilmes et al., 2009; Pitari et al., 2014), stratospheric dynamics (Aquila et al., 2014) and sea-ice extent (Berdahl et al., 2014). Precipitation changes could result from changes to the moist static stability of the atmosphere and a concomitant weakening of the hydrological cycle (Bala et al., 2008), and the regional precipitation changes under GeoMIP simulations have been shown to be reasonably consistent across a range of climate models (Tilmes et al., 2013). Ozone concentrations could change as a result of enhanced heterogeneous chemistry on the surface of sulfate aerosols or indirectly by changes to the stratospheric dynamics and chemistry (e.g. Tilmes et al., 2009). Stratospheric dynamical changes could occur as the result of tropical heating in the sulfate layer and by changes to wave propagation from the troposphere (e.g. Aquila et al., 2014).

In order to ameliorate the known side-effects of sulfate injection, some authors have proposed alternative aerosols to sulfate (e.g. Teller et al., 1997). Crutzen (2006) suggested the possible injection of black carbon (BC), which would mimic hypothetical nuclear winter scenarios. One advantage of BC over sulfate is that less mass would be needed for an equivalent radiative forcing (Crutzen, 2006). BC particles efficiently absorb solar radiation, unlike sulfate which primarily reflects solar radiation (Ferraro

Climatic impacts of stratospheric geoengineering with sulfate, black carbon and titania injection

A. C. Jones et al.

Title Page

Abstract

Introduction

Conclusions

References

Tables

Figures

◀

▶

◀

▶

Back

Close

Full Screen / Esc

Printer-friendly Version

Interactive Discussion

et al., 2011). Alternatively, minerals such as titania (TiO_2), silica (SiO_2) and alumina (Al_2O_3), which have a high refractive index at wavelengths of peak solar radiative flux (~ 550 nm), have also been suggested (Pope et al., 2012). Although the use of alternative aerosols is not a new suggestion (e.g. Teller et al., 1997), comparatively little research has been conducted on their potential utility. Kravitz et al. (2012) simulated a constant BC injection scenario of 1 Tgyr^{-1} in the tropics for small radius ($0.03 \mu\text{m}$) and large radius ($0.15 \mu\text{m}$) aerosols. They found that the small particle BC aerosol scenario produced a global surface cooling of -9.45°C , but also induced stratospheric warming $> +60^\circ\text{C}$ and global ozone loss of 50 %. The large particle BC aerosol scenario had a negligible climatic impact. Using a fixed dynamical heating (FDH) code, Ferraro et al. (2011) compared the stratospheric heating of sulfate, titania, and BC layers for an equivalent instantaneous radiative forcing. Their results showed a tropical stratospheric warming signal for all the aerosols, though much greater in the case of BC. To date, no work has used a comprehensive fully coupled atmosphere–ocean GCM to directly compare the possible climatic impacts of SAI with alternative aerosols to sulfate, which is the motivation for this research.

In this work, we simulate the stratospheric injection of sulfate, titania and BC against a baseline RCP8.5 concentrations scenario using a fully-coupled GCM. Titania is selected to represent an efficient light-scattering aerosol and BC is selected as a light-absorbing aerosol. RCP8.5 is selected to give a significant greenhouse effect against which to employ geoengineering, in order to distinguish the climatic impacts specific to each aerosol. We chose to inject aerosol at a sufficient rate to counterbalance the Top Of the Atmosphere (TOA) global/annual-mean Radiative Flux (TOA-RF) imbalance caused by increasing atmospheric GHGs. Our simulation design is similar to the G3 scenario of the Geoengineering Model Intercomparison Project (GeoMIP), which instead used the RCP4.5 concentrations scenario as its baseline and injected sulfate at a sufficient rate to counterbalance GHG radiative forcing (Kravitz et al., 2011). We analyse the climate changes in the 2090s with respect to a simulated historical period and discuss impacts on a wide range of meteorological parameters.

2 Model

2.1 The HadGEM2-CCS model

For this investigation, we use the HadGEM2-CCS climate model in a fully coupled atmosphere–ocean mode. HadGEM2-CCS is the high-top configuration of the HadGEM2 family of models, and includes a well-resolved stratosphere. The atmosphere component comprises 60 vertical levels extending to 84 km and a horizontal resolution of $1.25^\circ \times 1.875^\circ$ latitude by longitude respectively. The 40-level ocean component has a horizontal resolution of 1° by 1° from the poles to 30° N/S, with the latitudinal resolution then increasing smoothly to 0.33° at the equator (The HadGEM2 Development Team, 2011). For this investigation, GHG concentrations, stratospheric ozone, anthropogenic aerosols and aerosol precursor gases are prescribed following the Coupled Model Intercomparison Project phase 5 (CMIP5) (Taylor et al., 2012) protocol, with historical data from 1860–2005 and RCP8.5 concentrations from 2005–2100. HadGEM2-CCS contains the aerosol module Coupled Large-scale Aerosol Simulator for Studies in Climate (CLASSIC). The module’s sulfur cycle is described in detail in Bellouin et al. (2011). Briefly, it includes the oxidation of sulfur dioxide (SO_2) to sulfate aerosol in aqueous and gas phase reactions. Sulfate is represented by Aitken, accumulation and dissolved modes, with hygroscopic growth in the accumulation mode following d’Almeida et al. (1991). Aerosol size modes are represented by lognormal size-distributions with a prescribed dry-mode median radius (r_m) and geometric standard deviation (σ).

2.2 Stratospheric aerosol microphysical and optical properties

For this investigation, stratospheric sulfate is modelled using the *volc2* size-distribution from Rasch et al. (2008) for the sulfate accumulation mode, with $r_m = 0.376 \mu\text{m}$ and $\sigma = 1.25$; the relatively large r_m is chosen to reflect the high concentrations of SO_2

Climatic impacts of stratospheric geoengineering with sulfate, black carbon and titania injection

A. C. Jones et al.

Title Page

Abstract

Introduction

Conclusions

References

Tables

Figures

◀

▶

◀

▶

Back

Close

Full Screen / Esc

Printer-friendly Version

Interactive Discussion



injected in this experiment. Hygroscopic growth is parameterised following Deepak and Gerber (1983).

CLASSIC includes a tropospheric BC scheme with fresh, aged and in-cloud modes (Bellouin et al., 2011). We introduce an additional non-hygroscopic stratospheric BC component and prescribe a lognormal size-distribution with $r_m = 0.0118 \mu\text{m}$ and $\sigma = 2.0$, which is taken from tropospheric BC observations (Deepak and Gerber, 1983). We prescribe a density for BC of 1000 kg m^{-3} and take refractive indices from a World Meteorological Organisation report (Deepak and Gerber, 1983).

For stratospheric titania, we assume the non-hygroscopic lognormal size distribution of Pope et al. (2012) with $r_m = 0.045 \mu\text{m}$ and $\sigma = 1.8$. This size-distribution was selected to give the titania aerosol a high scattering efficiency, as shown by Pope et al. (2012). We prescribe a density for titania of 4230 kg m^{-3} (Pope et al., 2012), and for the refractive indices we follow Ferraro et al. (2011) and use the average of the extra-ordinary and ordinary values from Ribarsky (1984).

The specific absorption (k_{abs}) and scattering (k_{sca}) coefficients for sulfate (accumulation/dry-mode), titania and BC are plotted in Fig. 1 as a function of wavelength. For sulfate, the specific extinction coefficient (k_{ext}) at 500 nm of 3200 kg m^{-3} and single scattering albedo (ω_o) of 1 reflects the non-absorbing properties of sulfate. Although titania's 500 nm scattering efficiency ($k_{\text{sca}} = 3850 \text{ kg m}^{-3}$) is greater than sulfate's in this instance, titania additionally absorbs SW radiation ($k_{\text{abs}} = 2000 \text{ kg m}^{-3}$ at 250 nm, and $k_{\text{abs}} = 600 \text{ kg m}^{-3}$ at 500 nm) which can be explained by the band-theory of solids (Yang et al., 2003). Thus titania is partially absorbing. Our modelled BC efficiently absorbs SW radiation ($k_{\text{abs}} = 8300 \text{ kg m}^{-3}$ at 500 nm) but also produces a non-negligible SW scattering effect ($k_{\text{sca}} = 2500 \text{ kg m}^{-3}$ at 500 nm) which is comparable in magnitude to the equivalent scattering efficiency of both titania and sulfate. Therefore, to describe titania as an efficient light-scatterer and/or BC as an efficient light-absorber is an over-simplification.

Our choice of particle size and density will impact the aerosol's gravitational sedimentation rate and therefore its atmospheric residence time (the sedimentation rate is

Climatic impacts of stratospheric geoengineering with sulfate, black carbon and titania injection

A. C. Jones et al.

Title Page

Abstract

Introduction

Conclusions

References

Tables

Figures

◀

▶

◀

▶

Back

Close

Full Screen / Esc

Printer-friendly Version

Interactive Discussion

noted HIST) and the geoengineering experiments during the period 2090–2100, with an emphasis on different geographical patterns.

4 Results

4.1 Effectiveness at maintaining global mean TOA-RF and near surface temperature

Figure 3 shows the global/annual-mean TOA-RF imbalance and near-surface air temperature anomaly for the geoengineering and RCP8.5 simulations, with respect to the HIST period. For all of the geoengineering simulations we were able to maintain TOA-RF balance for the entirety of the 80 year period (Fig. 3a). For G3S, G3TiO₂ and G3BC, the TOA-RF was maintained within ± 0.21 , ± 0.18 and $\pm 0.20 \text{ W m}^{-2}$, respectively (1 standard deviation throughout the 2020–2100 period).

However, the near-surface global temperature response differs between the aerosols with a greater cooling effect for sulfate than for titania or BC. This is due to the absorption of radiation by BC (and a lesser extent the absorption by titania) heating the stratosphere which then increases the terrestrial longwave radiation entering the troposphere reducing the tropopause-RF. As noted in several Intergovernmental Panel on Climate Change reports (e.g. Ramaswamy et al., 2001; Forster et al., 2007), it is the global mean tropopause-RF rather than the TOA-RF that is proportional to global mean surface temperature changes. Further analysis of stratospheric temperature changes will be provided in Sect. 4.4.

4.2 Aerosol distribution

The time-averaged injection rates for the 2090s period are $14 \text{ Tg SO}_2 \text{ yr}^{-1}$, 5.8 and 0.81 Tgyr^{-1} for G3S, G3TiO₂ and G3BC, respectively. This SO₂ injection rate is approximately equivalent to 1 Mt. Pinatubo eruption per year (Dhomse et al., 2014).

Climatic impacts of stratospheric geoengineering with sulfate, black carbon and titania injection

A. C. Jones et al.

Title Page

Abstract

Introduction

Conclusions

References

Tables

Figures

◀

▶

◀

▶

Back

Close

Full Screen / Esc

Printer-friendly Version

Interactive Discussion



tal Panel on Climate Change 5th assessment report (IPCC AR5) (e.g. Fig. 12.7 from Collins et al., 2013). All of the SAI experiments show a global-mean precipitation reduction with respect to both HIST and RCP8.5 (Fig. 6f–h), which is due to the deceleration of the hydrological cycle and is a robust model response to SAI (e.g. Yu et al., 2015; Tilmes et al., 2013; Bala et al., 2008). The magnitude of the precipitation changes are greater for G3BC than for G3S or G3TiO₂; for instance, the global mean precipitation anomaly is $-0.26 \text{ mm day}^{-1}$ for G3BC compared to $-0.12 \text{ mm day}^{-1}$ for G3S and $-0.14 \text{ mm day}^{-1}$ for G3TiO₂. This is because the stratospheric heating in G3BC applies an additional LW forcing at the tropopause and TOA which must be ameliorated by additional SW absorption in order to maintain radiative balance (Ferraro et al., 2011). The troposphere is relatively transparent to SW radiation but absorbs efficiently in the LW spectrum, therefore the annual-mean surface radiative forcing in the G3BC experiment is greater (-10.2 W m^{-2}) than for G3S or G3TiO₂ (-5.1 and -6.06 W m^{-2} respectively – see Fig. S4 in the Supplement). Bala et al. (2008) showed that the magnitude of the precipitation response is dependent on the surface radiative imbalance; therefore the precipitation reduction is amplified in G3BC.

Figure 7 shows the JJA temperature (Fig. 7a–d) and precipitation (Fig. 7e–h) anomalies. In the G3S and G3TiO₂ scenarios, the temperature is effectively maintained at HIST levels (Fig. 7b and d). However, a slight bias towards high-latitude NH warming in G3S and G3TiO₂ results in a northward displacement of the Inter-Tropical Convergence Zone (ITCZ), which is exemplified by the Sahelian precipitation increase in Fig. 7f and h. This phenomenon was noted by Haywood et al. (2013) and has been observed after large hemispherically asymmetric volcanic eruptions (Oman et al., 2006). Although the general pattern of precipitation change is similar for the 3 SAI scenarios, G3BC again displays a greater drying signal, with 80 % of the total land area experiencing a JJA precipitation reduction in G3BC compared to 70 % for G3TiO₂, 57 % for G3S and 52 % for RCP8.5.

Figure 8 shows the DJF temperature (Fig. 8a–d) and precipitation (Fig. 8e–h) anomalies. The temperature reduction over Greenland in G3BC (Fig. 8c) is due to the signifi-

Climatic impacts of stratospheric geoengineering with sulfate, black carbon and titania injection

A. C. Jones et al.

Title Page

Abstract

Introduction

Conclusions

References

Tables

Figures

◀

▶

◀

▶

Back

Close

Full Screen / Esc

Printer-friendly Version

Interactive Discussion

icant decrease in downwelling SW radiation at the surface during the Arctic sea-ice formation season (September-October-November), which leads to a positive sea-ice albedo feedback and further localised cooling. This inference is corroborated by Fig. 9, which shows the Arctic DJF sea-ice extent in terms of the average DJF sea-ice boundary (the Antarctic DJF sea-ice extent is shown in Fig. S5 in the Supplement). The sea-ice boundary in G3BC (Fig. 9c) extends to well below Greenland, and the total sea-ice extent anomaly is $+1.72$ million km^2 which vastly exceeds the HIST standard deviation of ± 0.52 million km^2 . In comparison, the sea-ice extent anomaly of -11 million km^2 for RCP8.5 (Fig. 9a) marks a reduction by 43% of the total HIST sea-ice extent. Returning to Fig. 8, the poleward shift in the NH extratropical rain-belt over the Atlantic in RCP8.5 (Fig. 8e) is a robust result of GHG-induced global warming and is related to storm track displacement (Lombardo et al., 2015). This same response is evident in the geoengineering simulations (Fig. 8f–h), although to a much lesser extent in G3S and G3TiO₂.

4.4 Stratospheric changes

Figure 10 shows the zonal-mean temperature change as a function of latitude and altitude for the JJA and DJF seasons. The stratospheric cooling in conjunction with tropospheric warming in RCP8.5 (Fig. 10a and e) is a robust result of increasing GHG-concentrations (e.g. Schmidt et al., 2013). Aerosols directly affect temperature by absorbing radiation, and indirectly by scattering radiation and by ambient dynamical and chemical changes (Carslaw and Kärcher, 2006). Sulfate predominantly absorbs in the LW and near-infrared spectrum (Fig. 1a), therefore the stratospheric radiative heating in G3S is mostly confined to the tropical region, where the stratosphere is significantly colder than the underlying warm troposphere (Ferraro et al., 2011). In contrast, titania and BC absorb in both the SW and LW spectrum (Fig. 1b and c), and therefore preferentially warm the summer-hemisphere and tropical stratosphere, where solar radiation is most prevalent. G3BC produces the most significant warming effect, with an average stratospheric (15–50 km altitude) temperature increase of $+33$ °C and a maximum tem-

Climatic impacts of stratospheric geoengineering with sulfate, black carbon and titania injection

A. C. Jones et al.

Title Page

Abstract

Introduction

Conclusions

References

Tables

Figures

◀

▶

◀

▶

Back

Close

Full Screen / Esc

Printer-friendly Version

Interactive Discussion



beyond the hydrological perturbation expected for sulfate injection. The G3BC scenario displays a greater cooling at high-latitudes than the G3S and G3TiO₂ scenarios (Figs. 6–8), which comparatively exhibit a net tropical cooling. This raises the question of whether a combination of aerosols could potentially be injected to produce a zonally-homogeneous cooling if necessary. Although SAI with sulfate and titania effectively maintains the regional distribution of temperature at HIST levels, with a slight residual warming at high latitudes, the hydrological cycle decelerates substantially in all SAI scenarios which is exemplified by a global-mean reduction in precipitation. However, annual-minimum sea-ice extent in both hemispheres and global-mean thermosteric sea-level (Fig. S10 in the Supplement) is almost entirely maintained at HIST levels for all SAI scenarios.

It is important to note that the climate impacts described above are dependent on the optical properties of the aerosol, which are further dependent on the aerosol particle's size, shape, and composition (e.g. Kravitz et al., 2012). In this investigation, the dry-mode size distribution of the aerosol species is held constant, and hygroscopic growth is not represented in the BC and titania schemes, nor are the effects of internal mixing represented. The injection of aerosol into pre-existing aerosol layers would lead to larger particles through coagulation and condensation, which further alters the aerosol's optical properties. The actual size of the aerosol in an SAI scheme would therefore depend on the injection strategy (e.g. location/season) and the size and composition of the injected species (e.g. Carslaw and Kärcher, 2006; Heckendorn et al., 2009). Recent research from Heckendorn et al. (2009), Pierce et al. (2010), English et al. (2012), and Weisenstein et al. (2015) have highlighted the importance of representing aerosol growth in SAI simulations. A detailed assessment of the aerosol microphysics for sulfate, BC, and titania injection is not within the scope of this paper, but presents an important subject for future work.

We have used prescribed ozone fields in these simulations because representing stratospheric chemistry is prohibitively computationally expensive for the multiple centennial simulations performed here (The HadGEM2 development team, 2011). Kravitz

Climatic impacts of stratospheric geoengineering with sulfate, black carbon and titania injection

A. C. Jones et al.

Title Page

Abstract

Introduction

Conclusions

References

Tables

Figures

◀

▶

◀

▶

Back

Close

Full Screen / Esc

Printer-friendly Version

Interactive Discussion

et al. (2012) showed that BC injection could potentially result in global ozone depletion of $> 50\%$, therefore the chemistry changes in SAI could potentially exceed the importance of the physical changes in terms of climatic impacts (e.g. UV radiation at the surface). Tilmes et al. (2012) showed that SW-scattering by geoengineered sulfate could potentially compensate for ozone-loss by back-scattering UV radiation in the tropics, but that this effect was insufficiently compensatory at high latitudes. Their result was scenario-dependent; ozone loss due to heterogeneous chemistry is enhanced for smaller particles and in the presence of higher free-radical concentrations. Therefore, additional research is needed in order to understand the effects on atmospheric chemistry of injecting alternative aerosols.

Another important aspect of SAI which is comparatively under-researched is the potential for impacts on human health. Aerosol concentrations in the air near the surface are of interest because of potential human respiratory impacts (Robock, 2008). For instance, the USA's National Institute for Occupational Safety and Health (NIOSH) recommends a maximum exposure limit of 0.3 mg m^{-3} for ultrafine titania particles (Dankovic et al., 2011). In our simulations, the maximum 2090's near-surface air concentration of titania (e.g. Fig. 4) for land regions between $60^\circ \text{ S} - 60^\circ \text{ N}$ is 254 ng m^{-3} , which is of the order of 10^3 less than the NIOSH exposure limit. The equivalent maximum concentration anomalies of BC in G3BC and SO_4 in G3S are 10 and 1851 ng m^{-3} respectively. More work is needed to assess the potential impacts of SAI on air quality and human health.

Another thus far unmentioned aspect of this research is the potential for surface albedo modification by aerosol deposition. In particular, BC deposition on snow reduces the snow albedo through enhanced snow-melt and the coarsening of snow grains, which results in amplified high-latitude warming (Marks and King, 2013). HadGEM2-CCS does not include the BC-on-snow feedback; therefore we estimate it by comparing the deposition rates for 2090s G3BC with the historical period. Jiao et al. (2014) report that the simulated annual mean Arctic ($> 60^\circ \text{ N}$) BC deposition for the 2006–2009 period ranges from $13 - 35 \times 10^7 \text{ kg yr}^{-1}$ for the AEROCOM Phase II

Climatic impacts of stratospheric geoengineering with sulfate, black carbon and titania injection

A. C. Jones et al.

Title Page

Abstract

Introduction

Conclusions

References

Tables

Figures

◀

▶

◀

▶

Back

Close

Full Screen / Esc

Printer-friendly Version

Interactive Discussion



models. The annual mean Arctic BC deposition for the 2006–2009 period from our HadGEM2-CCS simulations is $23 \times 10^7 \text{ kg yr}^{-1}$, which is within the AEROCOM range. The annual mean Arctic BC deposition anomaly for the 2090s period in G3BC is $19.6 \times 10^7 \text{ kg yr}^{-1}$. Therefore, the effects of dirty snow in such an SAI scenario would likely be significant, which would have impacts on the distribution of temperature, particularly at high latitudes, potentially confounding some of our conclusions.

This research has highlighted potential climate impacts of injecting various stratospheric aerosols in order to ameliorate global warming. However, further research is needed to further assess the climatic impacts of stratospheric aerosol injection such as the impacts on ozone. Whilst research has shown SAI to be capable of averting certain climate changes such as surface-warming, SAI provides no amelioration for other climate impacts, such as ocean acidification. It is therefore important to note that the safest possible solution to avoiding the sort of climate change instantiated by (e.g.) Fig. 6a of this report is to effectively mitigate greenhouse-gas emissions.

Data sets

Data used to generate figures, graphs, plots and tables are freely available via contacting the lead author: aj247@exeter.ac.uk.

The Supplement related to this article is available online at [doi:10.5194/acpd-15-30043-2015-supplement](https://doi.org/10.5194/acpd-15-30043-2015-supplement).

Author contributions. A. C. Jones designed the experiments, performed the simulations, analysed the data, and wrote the manuscript with guidance and advice from J. M. Haywood and A. Jones.

Acknowledgements. The authors would like to thank Valentina Aquila for supplying AVHRR and SAGE data, and to Peter Cox, Angus Ferraro, David Keith and Alan Robock for helpful discussions. A. C. Jones was supported by a Met Office/NERC CASE (ref. 580 009 183) PhD

Climatic impacts of stratospheric geoengineering with sulfate, black carbon and titania injection

A. C. Jones et al.

Title Page

Abstract

Introduction

Conclusions

References

Tables

Figures

◀

▶

◀

▶

Back

Close

Full Screen / Esc

Printer-friendly Version

Interactive Discussion



Forster, P., Ramaswamy, V., Artaxo, P., Bernsten, T., Betts, R., Fahey, D. W., Haywood, J.,
Lean, J., Lowe, D. C., Myhre, G., Nganga, J., Prinn, R., Raga, G., Schulz, M., and Van Dor-
land, R.: Changes in atmospheric constituents and in radiative forcing, in: Climate Change
2007: The Physical Science Basis, Contribution of Working Group I to the Fourth Assessment
5 Report of the Intergovernmental Panel on Climate Change, edited by: Solomon, S., Qin, D.,
Manning, M., Chen, Z., Marquis, M., Averyt, K. B., Tignor, M., and Miller, H. L., Cambridge
University Press, Cambridge, UK, New York, NY, USA, 129–234, 2007.

Haywood, J. M., Jones, A., Clarisse, L., Bourassa, A., Barnes, J., Telford, P., Bellouin, N.,
Boucher, O., Agnew, P., Clerbaux, C., Coheur, P., Degenstein, D., and Braesicke, P.: Ob-
servations of the eruption of the Sarychev volcano and simulations using the HadGEM2
10 climate model, *J. Geophys. Res.*, 115, D21212, doi:10.1029/2010JD014447, 2010.

Haywood, J. M., Jones, A., Bellouin, N., and Stephenson, D.: Asymmetric forcing
from stratospheric aerosols impacts Sahelian rainfall, *Nat. Clim. Change*, 3, 660–665,
doi:10.1038/nclimate1857, 2013.

15 Heckendorn, P., Weisenstein, D., Fueglistaler, S., Luo, B. P., Rozanov, E., Schraner, M., Thoma-
son, L. W., and Peter, T.: The impact of geoengineering aerosols on stratospheric tempera-
ture and ozone, *Environ. Res. Lett.*, 4, 045108, doi:10.1088/1748-9326/4/4/045108, 2009.

International Civil Aviation Organisation (ICAO): Manual of the ICAO Standard Atmosphere:
Extended to 80 Kilometres (262 200 Feet), Doc 7488/3, 3rd edn., International Civil Aviation
20 Organization, Montreal, Quebec, p. 305, 1993.

Jiao, C., Flanner, M. G., Balkanski, Y., Bauer, S. E., Bellouin, N., Bernsten, T. K., Bian, H.,
Carslaw, K. S., Chin, M., De Luca, N., Diehl, T., Ghan, S. J., Iversen, T., Kirkevåg, A., Koch, D.,
Liu, X., Mann, G. W., Penner, J. E., Pitari, G., Schulz, M., Seland, Ø., Skeie, R. B., Steen-
rod, S. D., Stier, P., Takemura, T., Tsigaridis, K., van Noije, T., Yun, Y., and Zhang, K.: An
25 AeroCom assessment of black carbon in Arctic snow and sea ice, *Atmos. Chem. Phys.*, 14,
2399–2417, doi:10.5194/acp-14-2399-2014, 2014.

Kawatani, Y. and Hamilton, K.: Weakened stratospheric quasibiennial oscillation driven by in-
creased tropical mean upwelling, *Nature*, 497, 478–481, doi:10.1038/nature12140, 2013.

Kharin, V. V., Zwiers, F. W., Zhang, X., and Wehner, M.: Changes in temperature and precipita-
tion extremes in the CMIP5 ensemble, *Climatic Change*, 119, 345–357, doi:10.1007/s10584-
30 013-0705-8, 2013.

Climatic impacts of stratospheric geoengineering with sulfate, black carbon and titania injection

A. C. Jones et al.

Title Page

Abstract

Introduction

Conclusions

References

Tables

Figures

◀

▶

◀

▶

Back

Close

Full Screen / Esc

Printer-friendly Version

Interactive Discussion



Tegtmeier, S., Kruger, K., Wohltmann, I., Schoellhammer, K., and Rex, M.: Variations of the residual circulation in the Northern Hemispheric winter, *J. Geophys. Res.*, 113, D16109, doi:10.1029/2007JD009518, 2008.

Teller, E., Wood, L., and Hyde, R.: Global Warming and Ice Ages: I. Prospects for Physics-Based Modulation of Global Change, Lawrence Livermore National Laboratory Publication, 22nd International Seminar on Planetary Emergencies, Erice (Sicily), Italy, 20–23 August 1997, in preparation, UCRL-JC-128715, 18 pp., 1997.

The HadGEM2 Development Team: G. M. Martin, Bellouin, N., Collins, W. J., Culverwell, I. D., Halloran, P. R., Hardiman, S. C., Hinton, T. J., Jones, C. D., McDonald, R. E., McLaren, A. J., O'Connor, F. M., Roberts, M. J., Rodriguez, J. M., Woodward, S., Best, M. J., Brooks, M. E., Brown, A. R., Butchart, N., Dearden, C., Derbyshire, S. H., Dharssi, I., Doutriaux-Boucher, M., Edwards, J. M., Falloon, P. D., Gedney, N., Gray, L. J., Hewitt, H. T., Hobson, M., Huddleston, M. R., Hughes, J., Ineson, S., Ingram, W. J., James, P. M., Johns, T. C., Johnson, C. E., Jones, A., Jones, C. P., Joshi, M. M., Keen, A. B., Liddicoat, S., Lock, A. P., Maidens, A. V., Manners, J. C., Milton, S. F., Rae, J. G. L., Ridley, J. K., Sellar, A., Senior, C. A., Totterdell, I. J., Verhoef, A., Vidale, P. L., and Wiltshire, A.: The HadGEM2 family of Met Office Unified Model climate configurations, *Geosci. Model Dev.*, 4, 723–757, doi:10.5194/gmd-4-723-2011, 2011.

Tilmes, S., Garcia, R. R., Kinnison, D. E., Gettelman, A., and Rasch, P. J.: Impact of geoengineered aerosols on the troposphere and stratosphere, *J. Geophys. Res.*, 114, D12305, doi:10.1029/2008JD011420, 2009.

Tilmes, S., Kinnison, D. E., Garcia, R. R., Salawitch, R., Canty, T., Lee-Taylor, J., Madronich, S., and Chance, K.: Impact of very short-lived halogens on stratospheric ozone abundance and UV radiation in a geo-engineered atmosphere, *Atmos. Chem. Phys.*, 12, 10945–10955, doi:10.5194/acp-12-10945-2012, 2012.

Tilmes, S., Fasullo, J., Lamarque, J.-F., Marsh, D. R., Mills, M., Alterskjær, K., Muri, H., Kristjánsson, J. E., Boucher, O., Schulz, M., Cole, J. N. S., Curry, C. L., Jones, A., Haywood, J., Irvine, P. J., Ji, D., Moore, J. C., Karam, D. B., Kravitz, B., Rasch, P. J., Singh, C., Yoon, J.-H., Niemeier, U., Schmidt, H., Robock, A., Yang, S., and Watanabe, S.: The hydrological impact of geoengineering in the Geoengineering Model Intercomparison Project (GeoMIP), *J. Geophys. Res.-Atmos.*, 118, 11036–11058, doi:10.1002/jgrd.50868, 2013.

Weisenstein, D. K. and Keith, D. W.: Solar geoengineering using solid aerosol in the stratosphere, *Atmos. Chem. Phys. Discuss.*, 15, 11799–11851, doi:10.5194/acpd-15-11799-2015, 2015.

5 Yang, H., Zhu, S., and Pan, N.: Studying the mechanisms of titanium dioxide as ultraviolet-blocking additive for films and fabrics by an improved scheme, *J. Appl. Polym. Sci.*, 92, 3201–3210, 2004.

Yu, X., Moore, J. C., Cui, X., Rinke, A., Ji, D., Kravitz, B., and Yoon, J.-H.: Impacts, effectiveness and regional inequalities of the GeoMIP G1 to G4 solar radiation management scenarios, *Global Planet. Change*, 129, 10–22, doi:10.1016/j.gloplacha.2015.02.010, 2015.

Climatic impacts of stratospheric geoengineering with sulfate, black carbon and titania injection

A. C. Jones et al.

Title Page

Abstract

Introduction

Conclusions

References

Tables

Figures



Back

Close

Full Screen / Esc

Printer-friendly Version

Interactive Discussion



Climatic impacts of stratospheric geoengineering with sulfate, black carbon and titania injection

A. C. Jones et al.

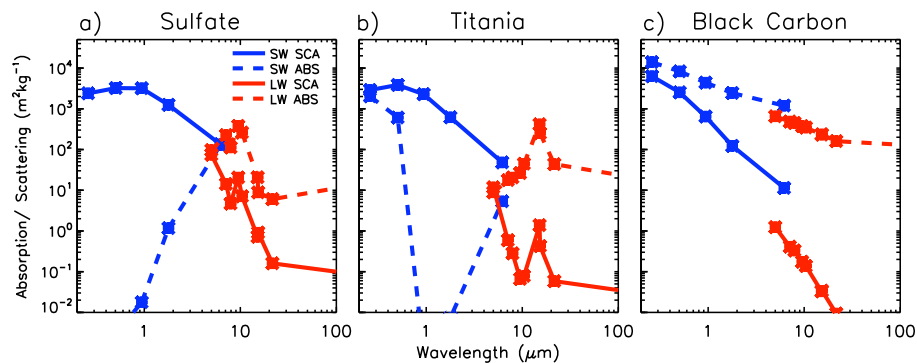


Figure 1. Optical properties as a function of wavelength for **(a)** accumulation-mode sulfate, **(b)** titania, **(c)** black carbon.

[Title Page](#)[Abstract](#)[Introduction](#)[Conclusions](#)[References](#)[Tables](#)[Figures](#)[◀](#)[▶](#)[◀](#)[▶](#)[Back](#)[Close](#)[Full Screen / Esc](#)[Printer-friendly Version](#)[Interactive Discussion](#)

Climatic impacts of stratospheric geoengineering with sulfate, black carbon and titania injection

A. C. Jones et al.

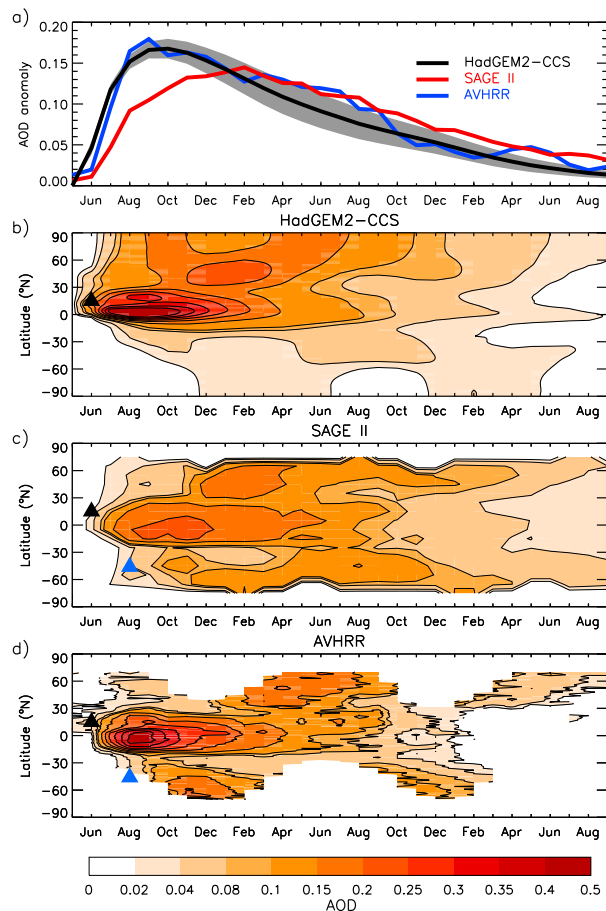


Figure 2. (a) 75° S–75° N-mean 550 nm sulfate AOD anomaly for the Pinatubo simulations and observations, (b–d) timeseries of zonal-mean 550 nm sulfate AOD anomaly.

Title Page

Abstract Introduction

Conclusions References

Tables Figures

◀ ▶

◀ ▶

Back Close

Full Screen / Esc

Printer-friendly Version

Interactive Discussion



Climatic impacts of stratospheric geoengineering with sulfate, black carbon and titania injection

A. C. Jones et al.

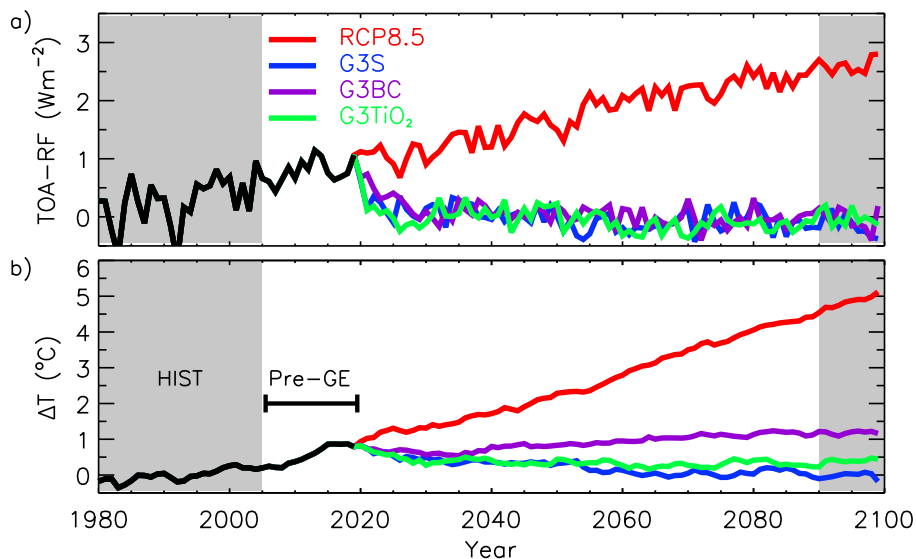


Figure 3. Timeseries of annual/global-mean (a) top-of-the-atmosphere radiative flux anomaly with respect to the pre-industrial control simulation (b) near-surface air temperature anomaly with respect to the HIST period.

[Title Page](#)[Abstract](#)[Introduction](#)[Conclusions](#)[References](#)[Tables](#)[Figures](#)[◀](#)[▶](#)[◀](#)[▶](#)[Back](#)[Close](#)[Full Screen / Esc](#)[Printer-friendly Version](#)[Interactive Discussion](#)

Climatic impacts of stratospheric geoengineering with sulfate, black carbon and titania injection

A. C. Jones et al.

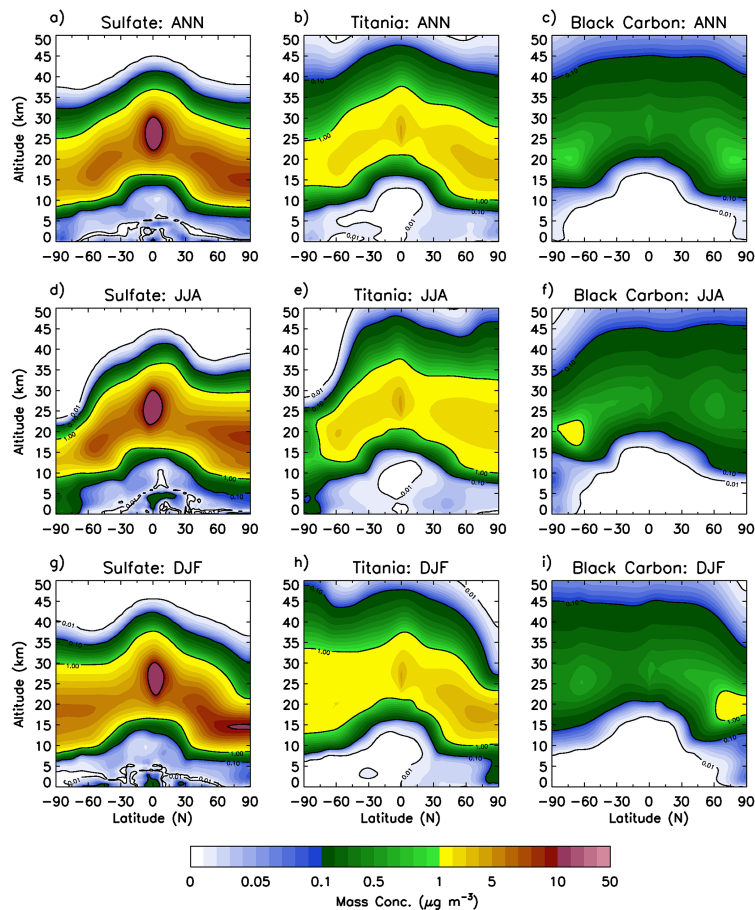


Figure 4. Annual and seasonal zonal-mean mass concentration anomalies for sulfate (G3S – left), titania (G3TiO₂ – centre) and black carbon (G3BC – right).

Climatic impacts of stratospheric geoengineering with sulfate, black carbon and titania injection

A. C. Jones et al.

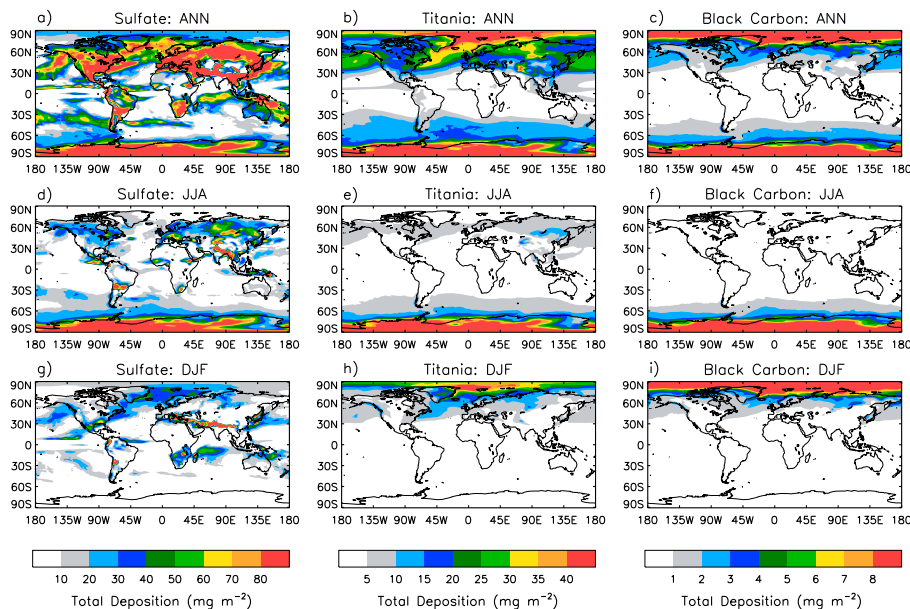


Figure 5. Annual and seasonal total deposition anomalies (in units of $\text{mg m}^{-2} \text{yr}^{-1}$ and $0.25 \times \text{mg m}^{-2} \text{yr}^{-1}$ respectively).

Title Page

Abstract

Introduction

Conclusions

References

Tables

Figures

◀

▶

◀

▶

Back

Close

Full Screen / Esc

Printer-friendly Version

Interactive Discussion



Climatic impacts of stratospheric geoengineering with sulfate, black carbon and titania injection

A. C. Jones et al.

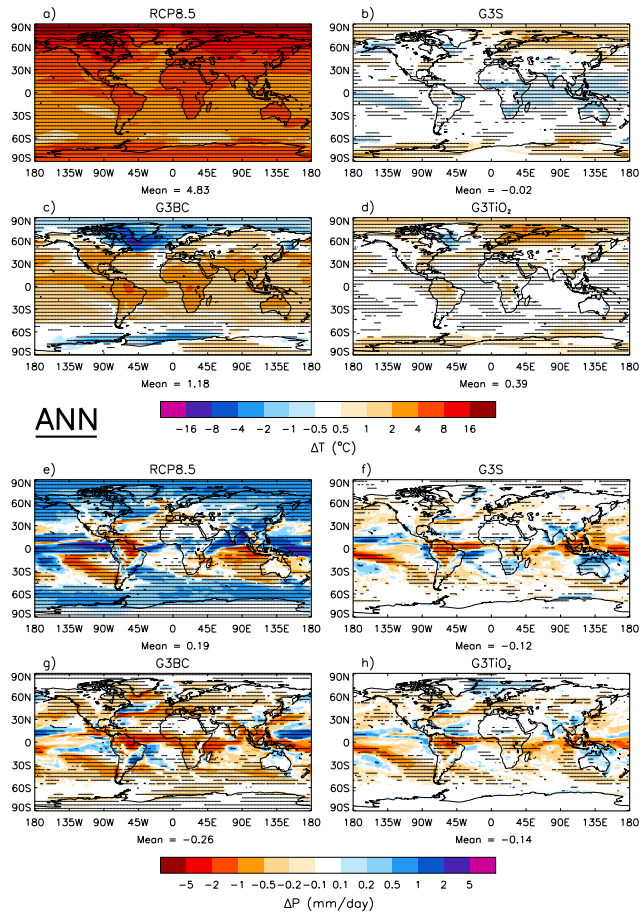


Figure 6. Annual-mean near-surface air temperature (top) and precipitation rate (bottom) anomalies with respect to HIST. Stippling indicates where changes are significant at the 5% level using a two-tailed Student's *t* test.

Title Page

Abstract Introduction

Conclusions References

Tables Figures

◀ ▶

◀ ▶

Back Close

Full Screen / Esc

Printer-friendly Version

Interactive Discussion

Climatic impacts of stratospheric geoengineering with sulfate, black carbon and titania injection

A. C. Jones et al.

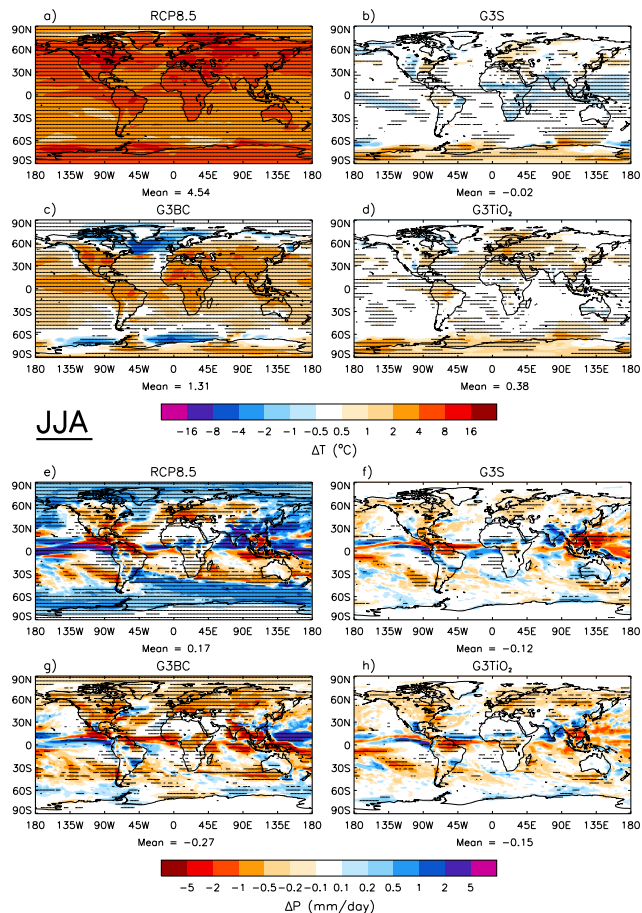


Figure 7. JJA near-surface air temperature (top) and precipitation rate (bottom) anomalies with respect to HIST.

Title Page

Abstract Introduction

Conclusions References

Tables Figures

◀ ▶

◀ ▶

Back Close

Full Screen / Esc

Printer-friendly Version

Interactive Discussion



Climatic impacts of stratospheric geoengineering with sulfate, black carbon and titania injection

A. C. Jones et al.

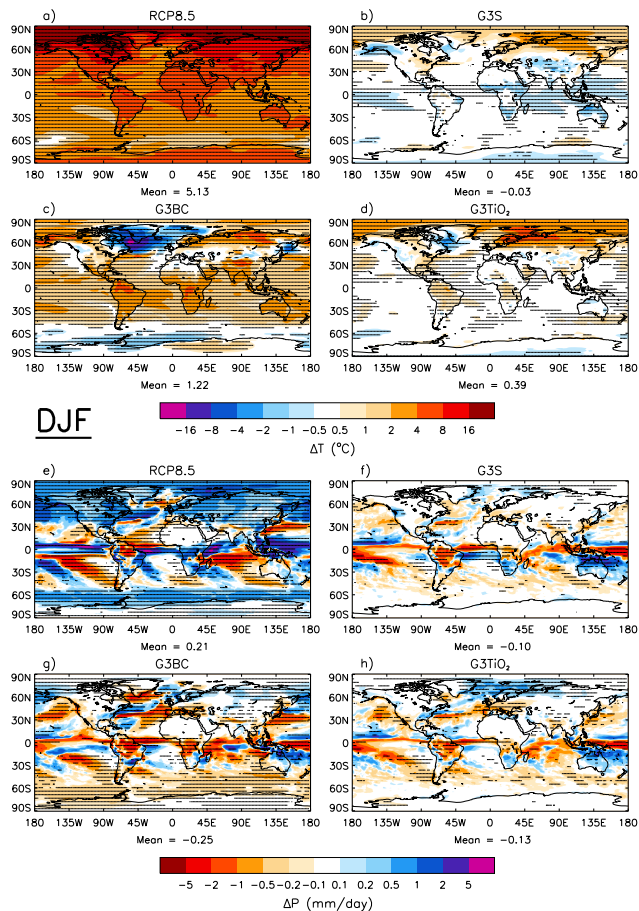


Figure 8. DJF near-surface air temperature (top) and precipitation rate (bottom) anomalies with respect to HIST.

Title Page

Abstract

Introduction

Conclusions

References

Tables

Figures

◀

▶

◀

▶

Back

Close

Full Screen / Esc

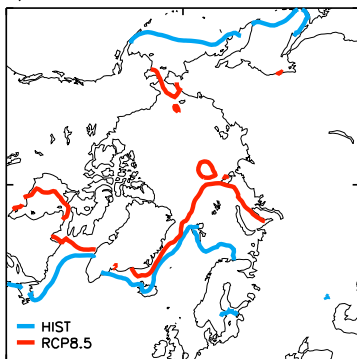
Printer-friendly Version

Interactive Discussion

Climatic impacts of stratospheric geoengineering with sulfate, black carbon and titania injection

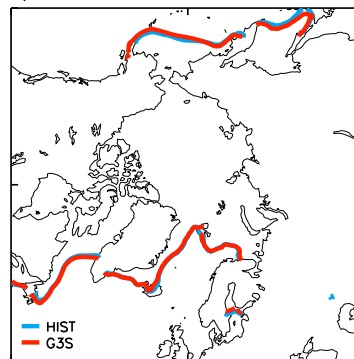
A. C. Jones et al.

a) RCP8.5: Sea-Ice DJF



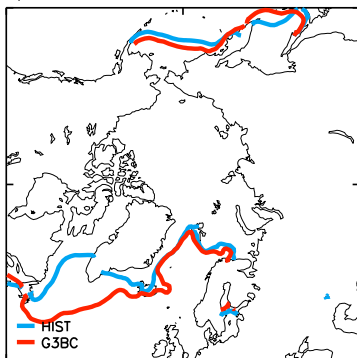
$$\Delta = -11.00 \text{ million km}^2$$

b) G3S: Sea-Ice DJF



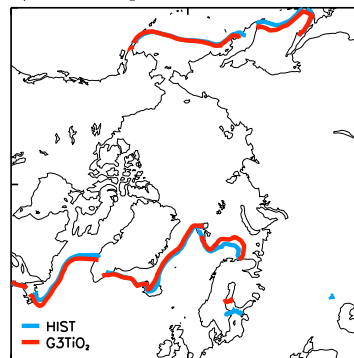
$$\Delta = -0.15 \text{ million km}^2$$

c) G3BC: Sea-Ice DJF



$$\Delta = +1.72 \text{ million km}^2$$

d) G3TiO₂: Sea-Ice DJF



$$\Delta = -0.39 \text{ million km}^2$$

Figure 9. DJF Northern Hemisphere sea-ice edge plotted with the HIST extent.

[Title Page](#)
[Abstract](#)
[Introduction](#)
[Conclusions](#)
[References](#)
[Tables](#)
[Figures](#)
[◀](#)
[▶](#)
[◀](#)
[▶](#)
[Back](#)
[Close](#)
[Full Screen / Esc](#)
[Printer-friendly Version](#)
[Interactive Discussion](#)

Climatic impacts of stratospheric geoengineering with sulfate, black carbon and titania injection

A. C. Jones et al.

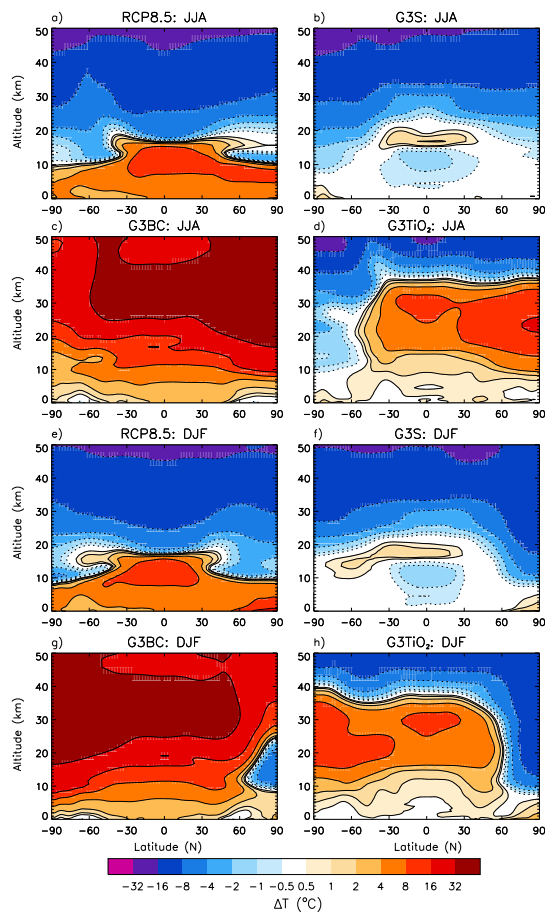


Figure 10. JJA (top) and DJF (bottom) zonal-mean temperature anomaly with altitude, with respect to HIST.

Climatic impacts of stratospheric geoengineering with sulfate, black carbon and titania injection

A. C. Jones et al.

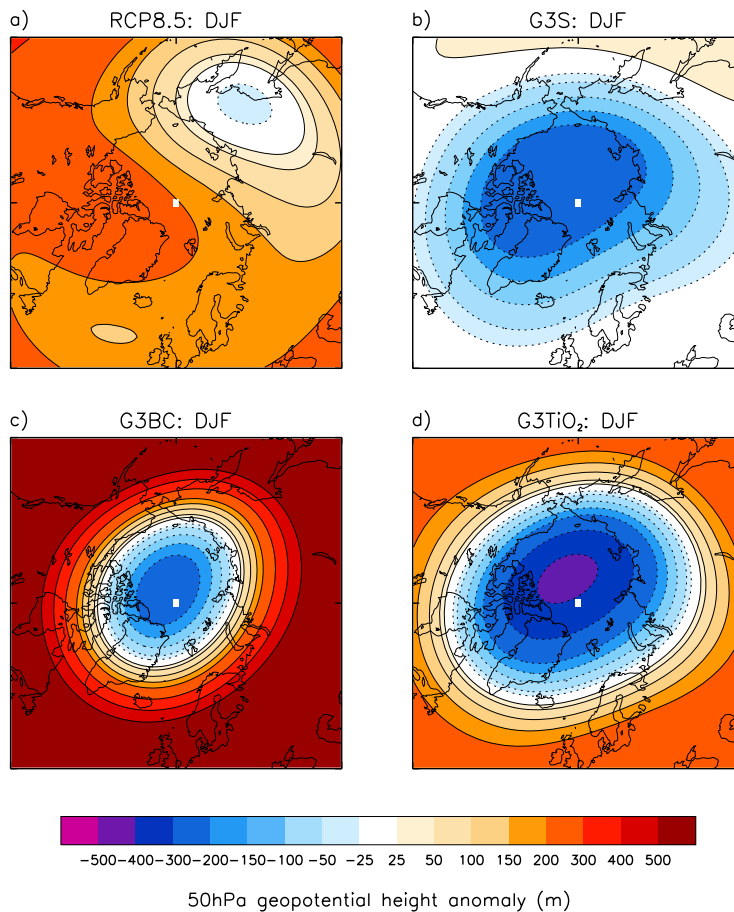


Figure 11. DJF 50hPa geopotential height anomaly.

Title Page

Abstract	Introduction
Conclusions	References
Tables	Figures

◀ ▶

◀ ▶

Back	Close
------	-------

Full Screen / Esc

Printer-friendly Version

Interactive Discussion



Climatic impacts of stratospheric geoengineering with sulfate, black carbon and titania injection

A. C. Jones et al.

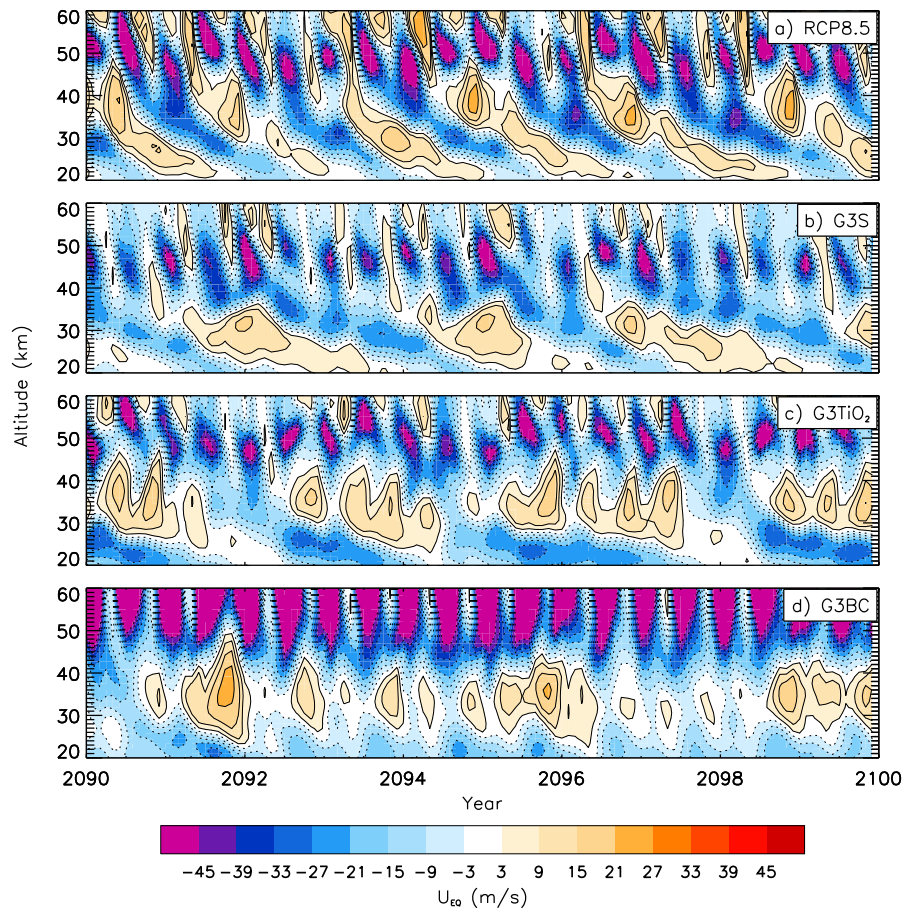


Figure 12. Timeseries of equatorial (5° S–5° N) zonal-mean zonal wind profile.

Title Page	
Abstract	Introduction
Conclusions	References
Tables	Figures
◀	▶
◀	▶
Back	Close
Full Screen / Esc	
Printer-friendly Version	
Interactive Discussion	

